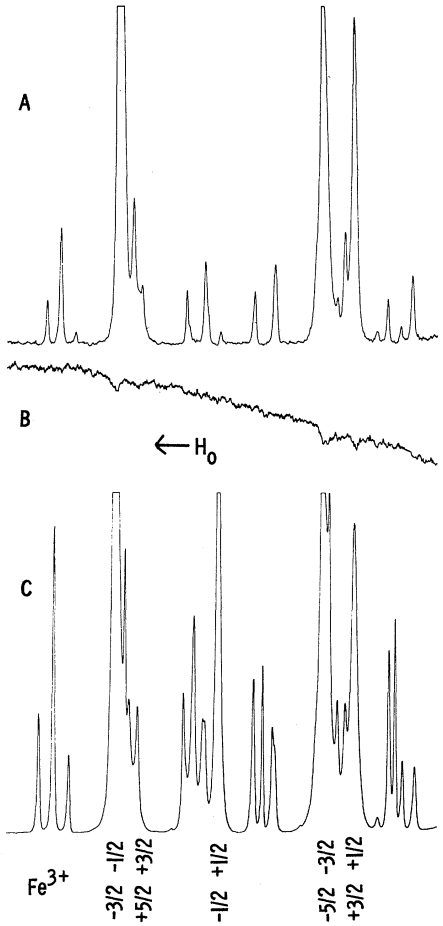


FIG. 3. $Fe^{3+}$ and $Mn^{2+}$ spectra in MgO (*not* an artist's tracing), taken by (a) *UUH* echoes, (b) ultrasonic absorption, and (c) *HH* echoes. $H_0$ approximately parallel to ⟨101⟩. $Fe^{3+}$ transitions are labeled; $Mn^{2+}$ similar but only the lowest-field hyperfine group is fully split. For a complete description of the spectra see Ref. 9.

tion spectrum. A spectrum taken with *HH* echoes is also shown. Note that the central $(+\frac{1}{2}, -\frac{1}{2})$ transitions of $Mn^{2+}$ are missing in the *UUH* spectrum, as dictated by quadrupolar spin selection rules. It is present, but small, in the $Fe^{3+}$ spectrum because with $H_0$ parallel to ⟨101⟩ there is a small admixture of other spin states. This illustrates how simultaneous measurements by both echo techniques complement each other in the identification of spectra.

We are investigating the possibility of observing stimulated echoes on $\Delta M = 2$ transitions by methods similar to the Raman echoes discussed by Hartmann.[10]

We wish to acknowledge discussions with Dr. G. Burns and Dr. D. Grischkowsky.

[1]E. L. Hahn, Phys. Rev. 77, 297 (1950).
[2]These rules may be easily deduced by expressing the times at which echoes form (as given, e.g., in Ref. 1) in terms of the retarded times of the pulses.
[3]I. D. Abella, N. A. Kurnit, and S. R. Hartmann, Phys. Rev. 141, 391 (1966).
[4]N. S. Shiren, Phys. Rev. Lett. 11, 3 (1963).
[5]E. L. Hahn, N. S. Shiren, and S. McCall, Phys. Lett. 37A, 265 (1971).
[6]N. S. Shiren, Phys. Rev. B 2, 2471 (1970).
[7]The spin phonon coupling constants, $G_{11}$, are (in units of $cm^{-1}$/unit strain) $Ni^{2+}$, 57; $Fe^{3+}$, 5; $Mn^{2+}$, 1.4. See G. D. Watkins and E. Feher, Bull. Amer. Phys. Soc. 7, 29 (1962); N. S. Shiren, Bull. Amer. Phys. Soc. 7, 29 (1962).
[8]S. R. P. Smith, F. Dravnieks, and J. E. Wertz, Phys. Rev. 178, 471 (1969), Eq. (24).
[9]W. J. Low, *Paramagnetic Resonance in Solids* (Academic, New York, 1960).
[10]S. R. Hartmann, IEEE J. Quantum Electron. 4, 802 (1968).

## Hyperchanneling, an Axial Channeling Phenomenon*

B. R. Appleton, C. D. Moak, T. S. Noggle, and J. H. Barrett
*Oak Ridge National Laboratory, Oak Ridge, Tennessee 37830*
(Received 31 January 1972)

We have studied the behavior of 21.6-MeV I ions undergoing proper axial channeling (hyperchanneling) in Ag. Ions of this special class traverse the crystal within a single axial channel and as a result exhibit conspicuously lower energy losses and an order of magnitude smaller acceptance angles than ordinary axially channeled ions. Analysis of the results indicates that hyperchanneled ions provide a new means for studying multiple scattering radiation damage, and ion-atom potentials in solids.

Detailed studies of the energy loss of 21.6-MeV I ions axially channeled in Ag single crystals show that over a small range of incidence angles with respect to [011] a distinct group of channeled ions exhibits unusually low energy losses. We identify this group as ions which remain within

a single axial channel throughout their history in the crystal. This interpretation is based on a model in which an ion is channeled provided its transverse energy relative to atom rows or planes is less than the repulsive continuum potential of the rows or planes. In planar channeling a channeled ion travels in a single channel between adjacent atomic planes, whereas in axial channeling the majority of channeled ions wander from one axial channel to another. Axially channeled ions of a limited class, however, have transverse energies less than the potential barrier between adjacent rows and accordingly are constrained to travel through the crystal in a single axial channel. These ions are expected to have at least two distinctive characteristics, a smaller acceptance angle than ordinary axial channeling and lower energy losses because they sample larger average impact parameters than ions which wander from channel to channel.

The constraint of ions to single axial channels was recognized in the early calculations of Robinson and Oen[1] and further treated by Lehmann and Leibfried.[2] The only reported measurements are those of Eisen,[3] who observed low-loss "tails" in axial energy loss distributions. He referred to this effect as proper channeling, in keeping with Lindhard's[4] classification of "any kind of oscillation within a channel" as proper channeling. However, according to such usage this phenomenon should be called proper axial channeling to distinguish it from planar channeling, all of which is proper. To provide a less cumbersome name and to avoid any implicit reference to other types of channeling as improper, we shall use the term *hyperchanneling*.

Hyperchanneling was studied using a beam of 21.6-MeV I ions collimated to $\leq 0.01°$ full width onto a 0.60-$\mu$m-thick [001] Ag crystal which had a mosaic spread of 0.05° full width at half-maximum.[5] The energy spectra of those ions transmitted within $\pm 0.012°$ of the incident beam direction were recorded with an energy resolution of 185 keV full width at half-maximum and normalized by a beam monitor system. Details of the experimental apparatus[6] and specimen preparation[5] were reported earlier. Some experimental results are shown in Fig. 1. The peak on the right, lying within a narrow angular range and centered on a $dE/dx$ value of 3.15 MeV/$\mu$m, is due to hyperchanneling. It should be emphasized that the angular extent of this series of spectra ($\pm 0.45°$) is well within the calculated critical angles for ordinary axial channeling (i.e., $\psi_{1/2}$

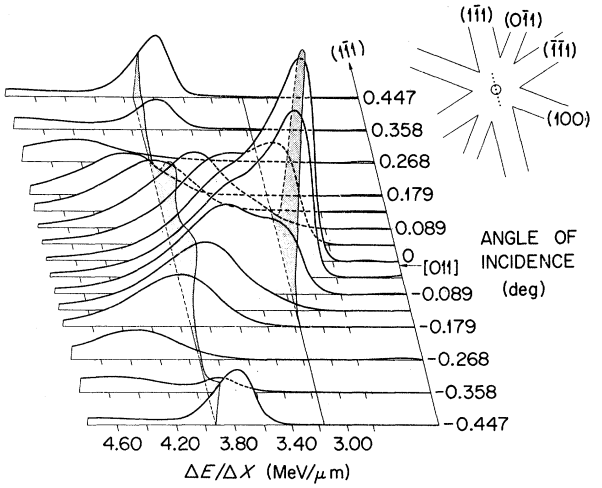


FIG. 1. Normalized energy loss distributions at various incidence angles to [011] for 21.6-MeV I ions transmitted through 0.85 $\mu$m of Ag. The insert shows the angular extent of the measurements (dotted line) and the hyperchanneling region (central circle). The widths shown for the planar channels are twice the half-angles calculated from Ref. 7.

$\sim 1.2°$ from Barrett[7] and $\psi_1 \sim 1.9°$ from Lindhard[4]). The major peaks in the energy loss distributions in Fig. 1 taken at $\pm 0.45°$ relative to [011] are nearly identical to those obtained at angles 5° to 10° from [011] in (1$\bar{1}$1). This indicates that when the beam is incident parallel to a low-index plane, many of the transmitted ions have distributions characteristic of planar channeling even at angles $\sim 0.25\psi_1$. As the incidence angle with respect to [011] is decreased, the energy loss distributions in Fig. 1 lose the characteristic {111} shape at about 0.30°, and a new group of ions with significantly lower energy losses is dominant within $\sim 0.12°$ of [011]. This low-loss group has the two characteristics expected of hyperchanneled ions. Related emergent patterns recorded photographically agree well with these spectra. Where planar energy losses are evident a characteristic elongated planar spot centered on the incident beam is observed superimposed on a ring of intensity centered on [011]. Within the range of hyperchanneling the ring has collapsed into an intense circular spot centered on [011].

The data were analyzed to determine a characteristic angle and absolute fraction for hyperchanneling. We estimate from the shapes of the population curves at various energy losses, such as those for 3.15 and 3.93 MeV/$\mu$m in Fig. 1, that only those ions with loss rates $\lesssim 3.7$ MeV/$\mu$m are hyperchanneled. The fraction of all ions

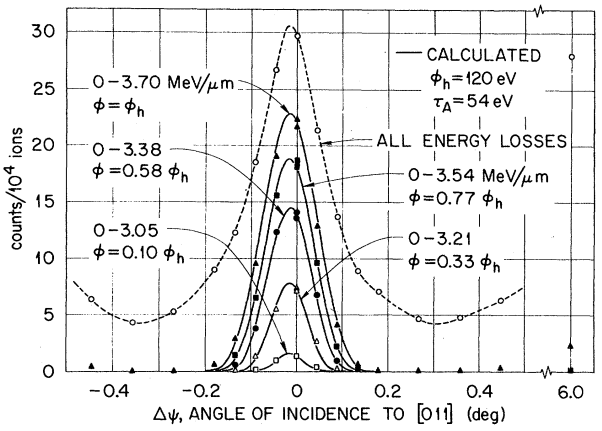


FIG. 2. Comparison of measured (data points) and calculated (solid lines) fractions of the beam reaching the detector as a function of angle of incidence to [011]. The dashed curve is not calculated but can be understood qualitatively in terms of emergent intensity distribution and detector geometry.

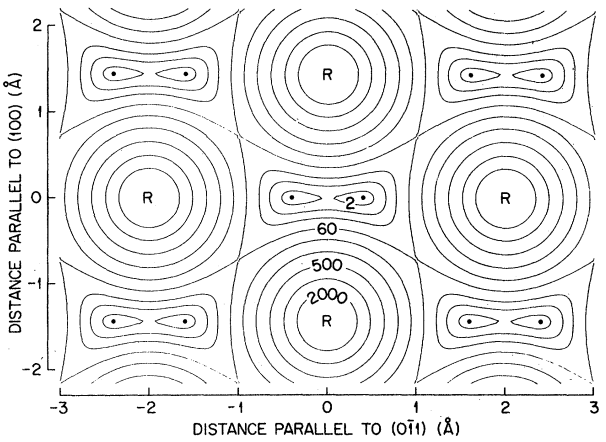


FIG. 3. Potential energy contours for I ions in the continuum potentials of [011] rows (*R*) of Ag atoms. All values are in eV and are relative to the minimum (dots), which has an absolute value of 72 eV.

recorded with energy losses below a specified value was extracted as a function of incidence angle and the results are the data points in Fig. 2.

The solid curves in Fig. 2 were calculated using the following model. As an ion of energy $E$ enters the crystal at an angle $\psi_i$ to the axial direction, it possesses a transverse kinetic energy $\tau_i = E\psi_i^2$. In addition, its entry point gives it a transverse potential energy $\varphi_i$ shown in the contours of Fig. 3. These were calculated using a potential determined by Robinson[8] from planar channeling experiments for 21.6–60-MeV I in Ag.[9] As the ion penetrates the crystal, it tends to traverse the entire space within the contour corresponding to its total transverse energy. We assume a crystal sufficiently thick for the ion to achieve statistical equilibrium over this contour, which implies that the probability of finding it is constant inside the contour and zero outside.[4] In moving through the crystal, the ion acquires additional transverse energy $\epsilon_a$ from multiple scattering by electrons, lattice vibrations, and defects. The values of $\epsilon_a$ for the trajectories bounded by a particular contour will have some distribution, which we assume to be exponential with mean value $\epsilon_A$.

The detector in the experiment has a small half-angle of acceptance $\psi_{det}$ and is located at an angle $\psi_0$ from the axial direction. The fraction of the beam reaching the detector is

$$F(\psi_0) = f_h \frac{\psi_{det}^2}{\psi_h^2}\left\{\ln\left(\frac{\varphi_h}{\epsilon_A}\right) - \ln\left(\frac{\tau_0}{\epsilon_A}\right) - \exp\left(\frac{\tau_0}{\epsilon_A}\right)\left[E_1\left(\frac{\tau_0}{\epsilon_A}\right) - E_1\left(\frac{\varphi_h}{\epsilon_A}\right)\right]\right\} \quad (1)$$

for $0 \leq \tau_0 \leq \varphi_h$ and zero otherwise. In Eq. (1), $\varphi_h = E\psi_h^2$ is the value of $\varphi$ midway between two rows in Fig. 3, $f_h$ is the fraction of area in the figure enclosed by the contour for $\varphi_h$, $\tau_0 = E\psi_0^2$, and $E_1$ is the exponential integral. We have used the fact that $\psi_i = \psi_0$ for our experiments and the approximation that the fraction of area within the contour for $\varphi$ is $(f_h/\varphi_h)\varphi$.

The probability that an ion reaches the detector is further influenced by beam divergence, contaminants on the crystal surface, and mosaic spread. In the present experiments we believe that mosaic spread is the dominant one of these three influences. Noting that the crystals used in the present experiments have mosaic spreads that are nearly Gaussian,[5] one may calculate a modified fraction $\bar{F}$ of ions reaching the detector,

$$\bar{F}(\psi_0) = \int_0^\infty \exp\left[-\frac{(\psi' - \psi_0)^2}{2\psi_M^2}\right] \exp\left(\frac{\psi_0\psi'}{\psi_M^2}\right) I_0\left(\frac{\psi_0\psi'}{\psi_M^2}\right) F(\psi') 2\psi' d\psi', \quad (2)$$

where $\psi_M = 0.022°$ is the variance of the mosaic spread and $I_0$ is a modified Bessel function.

Although present space does not permit it, flux peaking may also be treated by the same theoretical approach.

Values of all theoretical parameters except $\epsilon_A$ have been mentioned above. On the basis of observations for companion specimens, we believe defects make a negligible contribution to $\epsilon_A$. Using the work of Lindhard,[4,10] we conclude that the contribution of thermal vibrations is also negligible and estimate an upper limit from electron scattering of 6 eV for $\epsilon_A$.

In Fig. 3, $\varphi_h$ is 60 eV and $f_h$ is 0.30. Calculations using these values and other parameters measured and estimated above gave curves of $\bar{F}(\psi_0)$ that agreed qualitatively with the experimental data in Fig. 2 but had peaks about 3 times too high and were about 25% too narrow at the base. Varying $\varphi_h$ influenced only base width and $\epsilon_A$ only peak height, while $\psi_M$ influenced both. Values of 120 eV for $\varphi_h$ and 54 eV for $\epsilon_A$ provided the best fit to the 0–3.70-MeV/$\mu$m data in Fig. 2. The lower calculated curves were obtained by replacing $\varphi_h$ inside the braces of Eq. (1) by lower values of $\varphi$ to match the peak heights of the experimental data. Another possibility explored was that the parameters for mosaic spread, beam divergence, or surface layer scattering might be larger than we believe. If $\psi_M$ is used to adjust the base width, it must be doubled and $\epsilon_A$ must be 20–25 eV to get correct peak heights. Since all combinations of parameters that gave a good fit of theory to experiment have values of $\epsilon_A$ several times the estimated value, it appears that there is considerably more multiple scattering than is to be estimated for the mechanisms that we believe to be important. Such extra multiple scattering should also affect other experiments involving dechanneling rates. Our results also indicate that hyperchanneling investigations provide information on potentials in solids at impact parameters not accessible to other channeling experiments. The value of $\varphi_h$ used in calculating the solid curves in Fig. 2 is twice as large as the value obtained from the contours of Fig. 3. A factor that seems important here is the effect of lattice structure on the ion-atom potential, and a simple way of taking it into account is application of Wigner-Seitz rather than free-atom boundary conditions to the electron wave functions. Robinson[8,11] has examined the resulting potentials and finds that they differ only near the cell boundary where the Wigner-Seitz potential drops more rapidly. It appears that the Wigner-Seitz potential will give better agreement with the present experiments than the potential used in Fig. 3 and at the same time preserve agreement with earlier planar channeling experiments.[6,11-13]

Preliminary measurements indicate that hyperchanneling is about 2 orders of magnitude more sensitive to radiation damage than is ordinary axial channeling. This increased sensitivity arises because hyperchanneling is disrupted by angular deviations more than an order of magnitude smaller than those required for disruption of ordinary axial channeling.

In contrast to the pronounced hyperchanneled group in Fig. 1, [011] spectra of 3.0-MeV He in Au show only small leading edge shifts. Since $\varphi_h$ is about the same for these two cases, this is probably due to differences in the energy loss processes, multiple scattering, or damping.[4,14]

Calculations of $\varphi_h$ for some other axes and crystal structures suggest that compared to $[011]_{fcc}$, hyperchanneling conditions are probably more favorable for $[001]_{fcc}$, equally or more favorable for $[011]_{dia}$, $[001]_{dia}$, and $[001]_{bcc}$, and less favorable for $[111]_{bcc}$.

Some structure in the energy loss distributions of Fig. 1 is lost in the present analysis. Structure in these distributions appears to arise from a different source than in planar channeling experiments,[6,11-14] and we hope to present an analysis of it at a later date.

*Research sponsored by the U. S. Atomic Energy Commission under contract with the Union Carbide Corporation.

[1]M. T. Robinson and O. S. Oen, Phys. Rev. 132, 2385 (1963).

[2]C. Lehmann and G. Leibfried, J. Appl. Phys. 34, 2821 (1963).

[3]F. H. Eisen, Phys. Lett. 23, 401 (1966), and Can. J. Phys. 46, 561 (1968).

[4]J. Lindhard, Kgl. Dan. Vidensk. Selsk., Mat.-Fys. Medd. 34, No. 14 (1965).

[5]T. S. Noggle, in Proceedings of the Third International Symposium on Research Materials for Nuclear Measurements (to be published).

[6]S. Datz, C. D. Moak, T. S. Noggle, B. R. Appleton, and H. O. Lutz, Phys. Rev. 179, 315 (1969).

[7]J. H. Barrett, Phys. Rev. B 3, 1527 (1971).

[8]M. T. Robinson, in Proceedings of the Battelle Colloquium on Interatomic Potentials and Simulation of Lattice Defects, 14–19 June 1971 (to be published).

[9]T. S. Noggle, C. D. Moak, S. Datz, and B. R. Appleton, unpublished data.

[10]J. Lindhard, Kgl. Dan. Vidensk. Selsk., Mat.-Fys. Medd. 28, No. 8 (1954).

[11]M. T. Robinson, Phys. Rev. B 4, 1461 (1971).
[12]B. R. Appleton, S. Datz, C. D. Moak, and M. T. Robinson, Phys. Rev. B 4, 1452 (1971).
[13]F. H. Eisen and M. T. Robinson, Phys. Rev. B 4, 1457 (1971).
[14]M. T. Robinson, Phys. Rev. 179, 327 (1969).

# Crystal Field Splitting of Core $p_{3/2}$ Levels*

R. P. Gupta
*International Centre for Theoretical Physics, Trieste, Italy*

and

S. K. Sen
*Physics Department, University of Manitoba, Winnipeg, Canada*

(Received 27 March 1972)

The splittings of $p_{3/2}$ atomic core levels due to internal electric field gradients have been calculated for the case of $Tm^{3+}$ ions in thulium ethyl sulphate and shown to be measurable by electron spectroscopy. The splittings could be about 1 eV under favorable conditions.

It has been of great interest for quite some time to know about the effect of environment on the x-ray–emission linewidth in various transition elements. Recently, ESCA measurements[1] on some heavy elements in their compounds showed definite evidence of $p_{3/2}$ level splittings of the order of 10 eV.

We report here the calculations of various $p_{3/2}$ level splittings of thulium ions in thulium ethyl sulphate (TmES). The choice of TmES is due to simplicity of the calculations and the feasibility of comparison of a part of the results obtained here with Mössbauer-effect measurements.[2]

The quadrupolar part of the total Hamiltonian, representing the interaction between a point charge at $r$, $\theta$, and $\varphi$ with respect to the nucleus of the ion, and the crystalline electric potential as well as the electric potential due to the crystalline-electric-field– (CEF) split $4f$ unfilled shell could be written[2,3] (assuming axial symmetry of ligands surrounding the rare-earth ion),

$$H_Q = -[A_2^0 r^2 + \tfrac{1}{4}\langle J\|\alpha\|J\rangle\langle 3J_z^2 - J^2\rangle_T K(r)](3\cos^2\theta - 1), \quad (1)$$

where

$$K(r) = r^{-3}\int_0^r u_{4f}'^2 r'^2 dr' + r^2\int_r^\infty u_{4f}'^2 r'^{-3} dr',$$

with $u_{4f}'$ the radial part of the $4f$ wave function times $r'$; $\langle J\|\alpha\|J\rangle$ is the reduced matrix element; $\langle 3J_z^2 - J^2\rangle_T$ is the statistical average of matrix elements of the quadrupole operator equivalent between $2J+1$ CEF levels within a manifold of constant $\vec{J}$; and $A_2^0$ is the usual parameter in the crystal potential expansion. However, both terms in the interaction Hamiltonian are modified through their effect of polarization on the closed shells (Sternheimer effect[4]). The Sternheimer parameters pertinent to the second term $R_{np}$ have been calculated,[5] whereas those needed for the first term $\lambda_{np}$ are available in the literature.[3]

The energy splitting of the $np_{3/2}$ level corresponds to the difference in the expectation value of $H_Q$ between the states $|\frac{3}{2}, \pm\frac{3}{2}\rangle$ and $|\frac{3}{2}, \pm\frac{1}{2}\rangle$; after including the Sternheimer effect

$$\Delta E_{np_{3/2}} = [A_2^0\langle r^2\rangle_{np}(1-\lambda_{np}) + \tfrac{1}{4}\langle J\|\alpha\|J\rangle\langle 3J_z^2 - J^2\rangle_T\langle K(r)\rangle_{np}(1-R_{np})]$$
$$\times\langle\tfrac{3}{2}\|\alpha\|\tfrac{3}{2}\rangle(\langle\tfrac{3}{2}|3J_z^2 - J^2|\tfrac{3}{2}\rangle - \langle\tfrac{1}{2}|3J_z^2 - J^2|\tfrac{1}{2}\rangle). \quad (2)$$

Confining our attention to the $^3H_6$ term of the ground multiplet of TmES, we have evaluated $A_2^0 \equiv C_2^0/\langle r^2\rangle_{4f}(1-\lambda_{4f})$, where $C_2^0 = 130.5\ \mathrm{cm}^{-1}$ is obtained by Barnes *et al.*[2] from the optical measurements of Wong and Richman,[6] and $\langle r^2\rangle_{4f}(1-\lambda_{4f}) = 0.282$.[3] $\langle J\|\alpha\|J\rangle = 1.02\times10^{-2}$; $\langle 3J_z^2 - J^2\rangle_T$ are calculated using Table IV of Ref. 2. The factor outside the square bracket is $\frac{4}{5}$. The $R_{np}$ and $\langle K(r)\rangle_{np}$ pertinent to the present work